Krylov Subspace Methods for Harmonic Balanced Finite Element Methods

Herbert De Gersem[1]*, Stefan Vandewalle[2], and Kay Hameyer[1]

[1] Katholieke Universiteit Leuven, Dep. EE (ESAT) / Div. ELEN
Kardinaal Mercierlaan 94, B-3001 Leuven, Belgium
[2] Katholieke Universiteit Leuven, Dep. Computer Science
Celestijnenlaan 200A, B-3001 Leuven, Belgium

Abstract A Conjugate Gradient solver is developed for harmonic balanced finite element systems. This approach avoids the construction of real equivalent systems which suffer from worse spectral conditions for Krylov subspace solvers. The application to a transformer with ferromagnetic material shows the better convergence of the Conjugate Gradient solver.

1 Introduction

Alternating current electrical energy transducers in steady-state regime are commonly simulated by linearised time-harmonic finite element (FE) models. As phenomena at higher harmonics due to power electronic supply or ferromagnetic saturation have an increasing technical importance, transient FE or harmonic balanced FE (HBFEM) simulation is becoming more and more important. In the applications considered here, periodic steady-state operations are simulated. Since only a few, a priori known frequencies are technically relevant, multi-harmonic simulation is favoured over time stepping.

The use of HBFEM is not a very common practice, mainly because of the expensive solution of the corresponding matrix system. Previously published research and existing implementations rely upon a weakly coupled time-harmonic scheme [1] or a real-valued splitting of the system matrix [2]. Here, a different, strongly coupled approach without splitting is presented. The emphasis is on the development of appropriate Krylov subspace solvers for the particular systems of equations arising from this approach.

2 Finite Discrete Spectra

Consider a periodic signal $a(t)$ and its corresponding discrete spectrum $\underline{a}(\omega)$ with ω the pulsation. The period is t_1 and hence, the lowest participating frequency, besides the DC-component, is $f_1 = 1/t_1$. All other participating

* The authors are grateful to the Belgian "Fonds voor Wetenschappelijk Onderzoek Vlaanderen" (G.0427.98) and the Belgian Ministry of Scientific Research (IUAP No. P4/20) for the financial support of this work.

frequencies are multiples of f_1, i.e. $f_k = kf_1, k \in \mathbb{N}$. The corresponding pulsations are $\omega_k = 2\pi f_k$. The *harmonic component* of *harmonic order* k,

$$\underline{a}|_k = \underline{a}(\omega_k) = \frac{2}{T}\int_0^T a(t)e^{j\omega_k t}dt, \tag{1}$$

represents the magnitude of the discrete spectrum at pulsation ω_k (Fig. 1). *Even* and *odd harmonics* are distinguished by their even and odd orders respectively.

For particular applications, only a finite set of harmonics is present or technically relevant. The set is called a *harmonic pattern* and is denoted by $P = (p_1, p_2, \cdots)$ with $p_1, p_2, \cdots$ positive numbers indicating the orders of the considered harmonics. The *finite discrete spectrum* is denoted by $\underline{a} = (\underline{a}|_{p_1}, \underline{a}|_{p_2}, \cdots)$. This notation only gathers the complex coefficients corresponding to positive orders. Because $\underline{a}_{|_{-p}} = \overline{\underline{a}_{|_p}}$, only those have to be computed. All spectra $\underline{a}, \underline{b}, \cdots$ based on the same harmonic pattern P form a Hilbert space G_P, similar to $\mathbb{C}^{\#P}$ endowed with the inner product

$$(\underline{a}, \underline{b})_{G_P} = \sum_{p \in \pm P} \overline{\underline{a}}_{|_p} \underline{b}_{|_p}, \tag{2}$$

corresponding to the DC component of the convolution of $\underline{a}$ and $\underline{b}$, and the norm

$$\|\underline{a}\|_{G_P} = \sqrt{(\underline{a}, \underline{a})_{G_P}}. \tag{3}$$

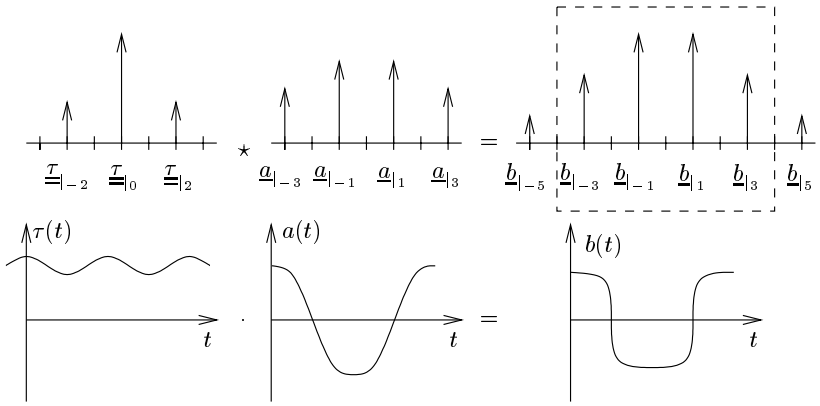

Figure1. Truncated convolution $\underline{\tau} \star \underline{a} = \underline{b}$.

3 Ferromagnetic Saturation

In the design of electrical energy transducers, ferromagnetic materials are applied because of their high permeabilities. The unwanted influence of saturation is kept acceptable by operating these materials at modest levels of saturation. As a consequence, the magnitudes of the field harmonics decrease considerably when the frequency increases. The discretisation of the frequency domain is straightforward:

- the periodicity of the excitation and the assumption that all materials are in steady-state behaviour, allows to consider only discrete spectra;
- technical considerations guide the selection of the harmonics to which the simulation is restricted.

The determination of the harmonic pattern can be done a priori and adaptively refined during the simulation. All excitating signals only contain odd harmonics. At higher amplitudes, saturation occurs and an infinite set of even harmonics is introduced in the pattern of the permeability. These excite additional harmonics in the magnetic field. In all examples here, the field quantities have the odd pattern $P = (1, 3, \cdots, 2n_h - 1)$ whereas the materials have the even pattern $Q = (0, 2, \cdots, 2n_h - 2)$, each of them considering n_h harmonic components. Spectra of field quantities are denoted by underlined, small roman characters whereas material spectra are represented by Greek symbols with double underlining.

4 Truncated Convolution

The convolution of a Q-patterned material coefficient with a P-patterned field quantity yields a field quantity with additional harmonic components. Successive convolutions increase the set of harmonics present in the field quantities. Hence, in practice, a truncated convolution is applied (Fig. 1):

$$\begin{array}{lll} \star : G_Q \times G_P \to G_P : \underline{\underline{\tau}} \star \underline{a} = (\underline{b}|_k) & & \\ \textit{with} \quad \underline{b}|_k = \sum_{p \in \pm P; q \in \pm Q; p+q=k} \underline{\underline{\tau}}|_q \underline{u}|_p & \text{if} \quad k \in P; & (4) \\ \underline{b}|_k = 0 & \text{if} \quad k \notin P. & \end{array}$$

Due to energy considerations, the truncated convolution of a material coefficient is a hermitian and positive definite operator with respect to $(\cdot, \cdot)_{G_P}$, i.e. $\forall \underline{a}, \underline{b} \in G_P$:

$$\left(\underline{\underline{\tau}} \star \underline{a}, \underline{b}\right)_{G_P} = \left(\underline{a}, \underline{\underline{\tau}} \star \underline{b}\right)_{G_P}; \tag{5}$$

$$\left(\underline{\underline{\tau}} \star \underline{a}, \underline{a}\right)_{G_P} \geq 0; \tag{6}$$

$$\left(\underline{\underline{\tau}} \star \underline{a}, \underline{a}\right)_{G_P} = 0 \Leftrightarrow \underline{a} = 0. \tag{7}$$

Consider e.g. $P = (1, 3)$ and $Q = (0, 2)$. Several matrix representations of the truncated convolution $\underline{\underline{\tau}} \star \underline{a} = \underline{b}$ are:

1. $$\begin{bmatrix} \tau_0 + \tau_2 \mathrm{Cg} & \overline{\tau}_2 \\ \tau_2 & \tau_0 \end{bmatrix} \begin{bmatrix} \underline{a}_{|_1} \\ \underline{a}_{|_3} \end{bmatrix} = \begin{bmatrix} \underline{b}_{|_1} \\ \underline{b}_{|_3} \end{bmatrix}; \tag{8}$$

2. $$\begin{bmatrix} \tau_0 & \tau_2 & & \\ \overline{\tau}_2 & \tau_0 & \tau_2 & \\ & \overline{\tau}_2 & \tau_0 & \tau_2 \\ & & \overline{\tau}_2 & \tau_0 \end{bmatrix} \begin{bmatrix} \underline{a}_{|_3} \\ \underline{a}_{|_1} \\ \underline{a}_{|_{-1}} \\ \underline{a}_{|_{-3}} \end{bmatrix} = \begin{bmatrix} \underline{b}_{|_3} \\ \underline{b}_{|_1} \\ \underline{b}_{|_{-1}} \\ \underline{b}_{|_{-3}} \end{bmatrix}; \tag{9}$$

3. $$\begin{bmatrix} \tau_0 & \mathrm{Re}\ \tau_2 & -\mathrm{Im}\ \tau_2 & \\ \mathrm{Re}\ \tau_2 & \tau_0 + \mathrm{Re}\ \tau_2 & \mathrm{Im}\ \tau_2 & \mathrm{Im}\ \tau_2 \\ -\mathrm{Im}\ \tau_2 & \mathrm{Im}\ \tau_2 & \tau_0 - \mathrm{Re}\ \tau_2 & \mathrm{Re}\ \tau_2 \\ & \mathrm{Im}\ \tau_2 & \mathrm{Re}\ \tau_2 & \tau_0 \end{bmatrix} \begin{bmatrix} \mathrm{Re}\ \underline{a}_{|_3} \\ \mathrm{Re}\ \underline{a}_{|_1} \\ \mathrm{Im}\ \underline{a}_{|_1} \\ \mathrm{Im}\ \underline{a}_{|_3} \end{bmatrix} = \begin{bmatrix} \mathrm{Re}\ \underline{b}_{|_3} \\ \mathrm{Re}\ \underline{b}_{|_1} \\ \mathrm{Im}\ \underline{b}_{|_1} \\ \mathrm{Im}\ \underline{b}_{|_3} \end{bmatrix} \tag{10}$$

where Cg, Re and Im are operators selecting the conjugate, real or imaginary parts of their arguments. Considering appropriate isomorphisms inbetween G_P and the vector spaces of the real equivalents, it is straightforward to prove (5), (6) and (7) using matrix calculus. The third notation is implemented in [2]. The second one is inefficient because of the combination of the double length and the complex type of the solution vectors. All three notations store superfluous copies of the material harmonics. In the approach presented here, the original formulation $\underline{\underline{\tau}} \star \underline{a} = \underline{b}$ is maintained. $\underline{a}$, $\underline{b}$ and $\underline{\underline{\tau}}$ are represented by appropriate software objects and hence avoiding splitting and additional copies. Notice that, in general, there is no $\underline{\underline{\tau}}^{-1}$ in G_Q such that

$$\underline{\underline{\tau}} \star \underline{a} = \underline{b} \Leftrightarrow \underline{\underline{\tau}}^{-1} \star \underline{b} = \underline{a}. \tag{11}$$

5 Harmonic Balanced Finite Element Method

The governing partial differential equation (PDE) is

$$\nabla \times (\nu \nabla \times \mathbf{A}) = \mathbf{J} \tag{12}$$

with $\mathbf{A}$ the magnetic vector potential, ν the reluctivity and $\mathbf{J}$ the current density. The PDE, transferred to the frequency domain, is

$$\nabla \times \left(\underline{\underline{\nu}} \star \nabla \times \underline{\mathbf{A}} \right) = \underline{\mathbf{J}}. \tag{13}$$

The time scale t is transformed into the pulsation scale ω. Even without parabolic term, this PDE captures the time-varying effects due to the alternating excitation and the reluctivity being non-linear and hence excitating higher harmonic components [3]. The geometry and excitation $\underline{\mathbf{J}} = (0, 0, \underline{J}_z)$ of the models, developed here, allow for a 2D nodal FE discretisation of the z-component of the magnetic vector potential $\underline{A}_z$ by n_f linear triangular FEs

N_i based upon a triangulation of the computational domain Ω. The resulting equation is

$$\mathcal{K}\underline{x} = \underline{f}, \tag{14}$$

expressing the relations

$$\sum_{j=1}^{n_f} \underline{\underline{k}}_{ij} \star \underline{x}_j = \underline{f}_i, \qquad i = 1, \cdots, n_f, \tag{15}$$

with

$$\underline{\underline{k}}_{ij} = \int_\Omega \underline{\underline{\nu}} \nabla N_i \cdot \nabla N_j d\Omega; \qquad \underline{f}_i = \int_\Omega \underline{J}_z N_i d\Omega; \qquad \underline{x}_j = \underline{A}_{zj}. \tag{16}$$

$\underline{x}$ and $\underline{f}$ are elements of $G_P^{n_f \times 1}$. $\mathcal{K}$ is an operator mapping $G_P^{n_f \times 1}$ into $G_P^{n_f \times 1}$. In practice, $\mathcal{K}$ is represented by an $n_f \times n_f$ sparse matrix of coefficients $\underline{\underline{k}}_{ij} \in G_Q$. The definitions of the inner product and norm for G_P extend in the classical way to $G_P^{n_f \times 1}$:

$$(\underline{u}, \underline{v})_{G_P^{n_f \times 1}} = \sum_{i=1}^{n_f} (\underline{u}_i, \underline{v}_i)_{G_P}; \tag{17}$$

$$\|\underline{u}\|^2_{G_P^{n_f \times 1}} = \sum_{i=1}^{n_f} \|\underline{u}_i\|^2_{G_P}. \tag{18}$$

6 Conjugate Gradients for HBFEM

The operator $\mathcal{K}$ is hermitian and positive definite with respect to (17). This is easily proved using (5), (6) and (7) together with the properties of the discretised diffusion operator. The method of choice for solving such a system is Conjugate Gradients (CG) [4]. The symmetry enables the application of the Lanczos algorithm to construct the Krylov subspace

$$\mathrm{K}_m(\underline{r}_0, \mathcal{K}) = \mathrm{span}\left\{\underline{r}_0, \mathcal{K}\underline{r}_0, \cdots, \mathcal{K}^{m-1}\underline{r}_0\right\} \tag{19}$$

by a three-terms recurrence relation

$$\mathcal{K}\underline{V}_m = \underline{V}_{m+1}\widetilde{T}. \tag{20}$$

$\underline{V}_m \in G_P^{n_f \times m}$ collects the base vectors of $\mathrm{K}_m(\underline{r}_0, \mathcal{K})$. $\widetilde{T} \in \mathbb{C}^{(m+1)\times m}$ is a tridiagonal matrix of recurrence coefficients. Its type is complex because the inner product (2) maps two finite discrete spectra onto $\mathbb{C}$. The positive definite $\mathcal{K}$ defines the norm

$$\|\underline{v}\|_{\mathcal{K}} = (\mathcal{K}\underline{v}, \underline{v})_{G_P^{n_f \times 1}} \tag{21}$$

with respect to which a new CG-approximant for $\underline{x}$ is computed. The classical CG algorithm is endowed with the operator $\mathcal{K}$ and the inner product (17).

The convergence of Krylov subspace solvers is poor unless preconditioning is applied to improve the spectral properties of the system [4]. A considerable improvement is achieved by diagonal scaling. Explicit scaling is only possible with scalars as, in general, $\underline{\underline{k}}_{ii}^{-1}$, and hence $\underline{\underline{k}}_{ii}^{-1} \star \underline{\underline{k}}_{ij} \star \underline{\underline{k}}_{jj}^{-1}$ do not exist within G_Q. Implicit scaling, i.e. solving $\underline{\underline{k}}_{ii} \star \underline{z}_i = \underline{r}_i, \quad i = 1, \cdots, n_f$ within the CG process, is efficiently performed by a modified Levinson algorithm [5]. This techniques are extended to a Symmetric Successive Overrelaxation (SSOR) preconditioner as well.

7 Implementation

Preconditioned CG involves 1 preconditioning step, 1 matrix-vector convolution, a few vector inner products and a few vector updates. These operations are considerably more expensive when compared to static, time-harmonic or transient simulation because of the convolutions. An efficient implementation is not straightforward: convolutions of relatively small spectra do not make optimal use of the available cache memory. Computer architectures are more adapted to vector products than convolutions. The implementation of the matrix-vector convolution as such, results in bad performing code. The implementation as a convolution of matrix-vector products, is 10 times faster (Table 1). The same is a fortiori true for the preconditioning step. The implementation of e.g. SSOR in such a way, is however much more cumbersome. Notice that reversing the order of processing only affects the implementation and does not change the system that is solved.

8 Real Equivalent Systems

The matrix elements, split up in their real equivalents (10), form a real-valued system of dimension $2n_f n_h$. The spectrum is real and positive but counts twice as much eigenvalues when compared to the original system. Moreover, as it includes, and hence embraces, the original spectrum, it is less favourable for Krylov subspace solvers. A worse convergence of CG is observed.

9 Application

A single-phase transformer, featuring a ferromagnetic, laminated iron core, is excited by pure sinusoidal currents at the frequency f_1. Hysteresis effects are neglected. The FE simulation of the magnetic field applies adaptive mesh refinement to achieve a prescribed accuracy. The a-posteriori error estimator applies the stored magnetic energy and the curvature of the magnetic flux lines per element as indicators for the refinement. The non-linearity of (14) is

resolved by a Picard iteration. Inbetween the successive steps k, adaptive underrelaxation is indispensable to ensure global convergence. The new iterate is

$$\underline{x}^{(k+1)} = \gamma \underline{\tilde{x}} + (1-\gamma)\underline{x}^{(k)} \tag{22}$$

where $\underline{\tilde{x}}$ is the solution of $\mathcal{K}^{(k)}\underline{\tilde{x}} = \underline{f}^{(k)}$ and the underrelaxation factor γ is chosen from $1, 0.5, 0.25, 0.125, 0.625$ minimising

$$\|\underline{f}^{(k+1)} - \mathcal{K}^{(k+1)}\underline{x}^{(k+1)}\|_{G_P^{n_f \times 1}}. \tag{23}$$

The updated spectrum $\underline{\underline{\nu}}^{(k+1)}$ follows from the application of the material characteristic in the time domain.

The solution is plotted for each harmonic component of the magnetic flux density separately (Fig. 3). Significant saturation and hence induction of higher harmonic fields, occur at the corners of the laminations. The convergences of CG applied to the original system and to its real equivalent, corresponding to the second refinement step and the third Picard step, are compared in Table 1 and Fig. 2. The mesh has 2201 nodes. 8 harmonic components are considered. CG applied to the system scaled by a scalar is denoted by CG*. The better spectral conditions of the original system is reflected in the smaller numbers of iteration steps and in the fact that CG still reaches convergence where CG applied to the real equivalent stagnates. The considerably more expensive matrix-vector multiplication and SSOR preconditioning in the case of CG for HBFEM causes these advantages not always to result in smaller computation times.

Table1. Timings (s) and iterations counts (between brackets) for the straightforward (str) and enhanced (enh) implementations of (SSOR)CG(*) applied to the HBFEM system of equations and its real equivalent system (real eq).

solver	HBFEM(str)	HBFEM(enh)	real eq
CG	318.73 (4841)	32.55 (4841)	-
CG*	58.12 (841)	5.45 (839)	-
SSORCG*	100.85 (291)	10.90 (287)	6.45 (327)

10 Conclusions

The system corresponding to a harmonic balanced finite element discretisation of a diffusion equation is positive definite and symmetric with respect to the proper inner product of the vector space of finite discrete spectra. Hence, the Conjugate Gradient method is applicable. This approach outperforms the solution of real equivalent systems because of their worse spectra. Attention has to be paid to an efficient implementation of the matrix-vector convolution and the preconditioning. The application to a single-phase transformer with ferromagnetic materials illustrates the benefits of this approach.

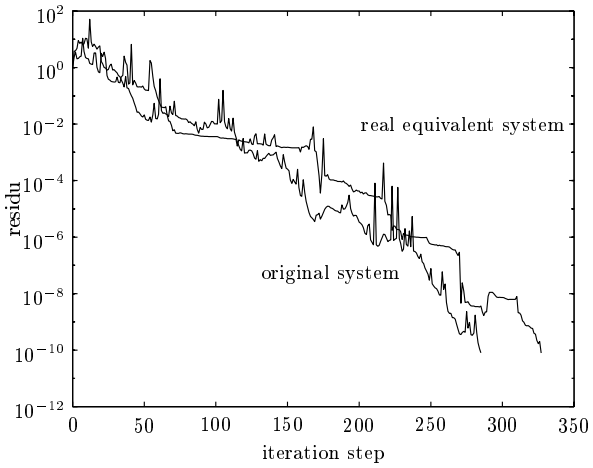

Figure2. Comparison of the convergence of SSORCG applied to the original and the real equivalent systems.

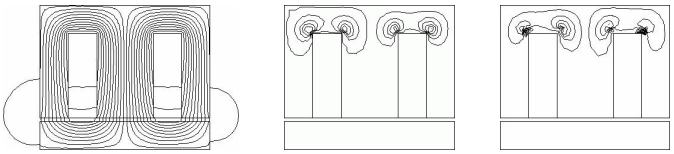

Figure3. 1st, 3rd and 5th harmonic of the magnetic flux density in a single-phase transformer.

References

1. J. Driesen, G. Deliége, T. Van Craenenbroeck, and K. Hameyer. Implementation of the harmonic balance fem method for large-scale saturated electromagnetic devices. In *Software for Electrical Engineering and Analysis and Design IV*, pages 75–84. WIT Press, 1999.
2. S. Yamada, K. Bessho, and J. Lu. Harmonic balance finite element method applied to nonlinear ac magnetic analysis. *IEEE Transactions on Magnetics*, 25(4):2971–2973, July 1989.
3. L. Vandevelde and J.A.A. Melkebeek J.J.C. Gyselinck. Steady-state finite element analysis in the frequency domain of inverter-fed squirrel cage induction motors. In *Proceedings of SPEEDAM94*, pages 29–34, Taormina, Italy, June 1994.
4. Y. Saad. *Iterative Methods for Sparse Linear Systems.* PWS Publishing Company, Boston, 1996.
5. G.H. Golub and C.F. Van Loan. *Matrix Computations.* The John Hopkins University Press, Baltimore, 1989.